THE JOURNAL OF BIOLOGICAL CHEMISTRY VOL. 285, NO. 33, pp. 25296–25307, August 13, 2010

In Silico Docking and Electrophysiological Characterization of Lacosamide Binding Sites on Collapsin Response Mediator Protein-2 Identifies a Pocket Important in Modulating Sodium Channel Slow Inactivation*[S]

Received for publication, April 23, 2010, and in revised form, May 28, 2010 Published, JBC Papers in Press, June 9, 2010, DOI 10.1074/jbc.M110.128801

Yuying Wang[‡1], Joel M. Brittain[§1], Brian W. Jarecki[‡1,2], Ki Duk Park[¶], Sarah M. Wilson[§], Bo Wang[§‖‡‡], Rachel Hale[‡], Samy O. Meroueh[§‖**‡‡], Theodore R. Cummins[‡§], and Rajesh Khanna[‡§3]**

*From the Departments of [‡]Pharmacology and Toxicology, [‖]Chemistry, and **Biochemistry and Molecular Biology, the [‡‡]Center for Computational Biology and Bioinformatics, and [§]Program in Medical Neuroscience, Paul and Carole Stark Neurosciences Research Institute, Indiana University School of Medicine, Indianapolis, Indiana 46202 and the [¶]Division of Medicinal Chemistry and Natural Products, Eshelman School of Pharmacy, University of North Carolina, Chapel Hill, North Carolina 27599*

The anti-epileptic drug (*R*)-lacosamide ((2*R*)-2-(acetylamino)-*N*-benzyl-3-methoxypropanamide (LCM)) modulates voltage-gated sodium channels (VGSCs) by preferentially interacting with slow inactivated sodium channels, but the observation that LCM binds to collapsin response mediator protein 2 (CRMP-2) suggests additional mechanisms of action for LCM. We postulated that CRMP-2 levels affects the actions of LCM on VGSCs. CRMP-2 labeling by LCM analogs was competitively displaced by excess LCM in rat brain lysates. Manipulation of CRMP-2 levels in the neuronal model system CAD cells affected slow inactivation of VGSCs without any effects on other voltage-dependent properties. *In silico* docking was performed to identify putative binding sites in CRMP-2 that may modulate the effects of LCM on VGSCs. These studies identified five cavities in CRMP-2 that can accommodate LCM. CRMP-2 alanine mutants of key residues within these cavities were functionally similar to wild-type CRMP-2 as assessed by similar levels of enhancement in dendritic complexity of cortical neurons. Next, we examined the effects of expression of wild-type and mutant CRMP-2 constructs on voltage-sensitive properties of VGSCs in CAD cells: 1) steady-state voltage-dependent activation and fast-inactivation properties were not affected by LCM, 2) CRMP-2 single alanine mutants reduced the LCM-mediated effects on the ability of endogenous Na^+ channels to transition to a slow inactivated state, and 3) a quintuplicate CRMP-2 alanine mutant further decreased this slow inactivated fraction. Collectively, these results identify key CRMP-2 residues that can coordinate LCM binding thus making it more effective on its primary clinical target.

The novel antiepileptic drug lacosamide ((*R*)-*N*-benzyl 2-acetamido-3-methoxypropionamide) (LCM,[4] Vimpat®) (1) has been recently approved in the U.S. and Europe for adjunctive treatment of partial-onset seizures in adults (2–4) and can be effective in cases of refractory epilepsy (5). Experimental data suggest two modes of action. Electrophysiology experiments in neuroblastoma cells proposed that lacosamide selectively enhanced sodium channel slow inactivation in a time- and voltage-dependent manner without affecting fast inactivation (6). Lacosamide shifted the slow inactivation voltage curve to more hyperpolarized potentials and enhanced the maximal fraction of channels that were slowly inactivated. The slow inactivation process by lacosamide was stereoselective, with only the (*R*)-stereoisomer being active. We also recently showed that lacosamide seems to enhance slow inactivation of voltage-gated Na^+ currents, a pharmacological action relevant in the hyperexcitable neuron (7). If true, lacosamide would be the only known antiepileptic agent to selectively modulate this property; however, this mechanism needs to be validated. This ability to preferentially block the electrical activity of neurons that are chronically depolarized compared with those at more normal resting potentials sets LCM apart from classic VGSC-targeted anti-epileptic drugs such as carbamazepine, phenytoin, and lamotrigine (7). In addition, protein pulldown assays and a combined chemical-proteomics approach have provided evidence that lacosamide interacts with collapsin response mediator protein 2 (CRMP-2), an axonal growth and guidance protein (8, 9). The role of CRMP-2 in the action(s) of lacosamide is not known.

CRMPs (also known as *UNC-33*-like proteins (Ulip), dyhydropyriminidase-related protein (DRP), TOAD (turned on after division), and TUC (TOAD/Ulip/DRP)), are a family of five intracellular phosphoproteins implicated in neurite outgrowth and axonal guidance (10–12). Although highest during

* This work was supported, in whole or in part, by National Institutes of Health Grants CA135380 (to S. O. M.) and NS053422 (to T. R. C.). This work was also supported by a grant from the Indiana State Dept. of Health (A70-9-079138, to R. K.), Spinal Cord and Brain Injury Fund (2286501, to R. K.).

[S] The on-line version of this article (available at http://www.jbc.org) contains supplemental Figs. S1–S3 and Table S1.

[1] These authors contributed equally to this work.

[2] Current address: Dept. of Physiology, University of Wisconsin-Madison Medical School, Madison, WI 53706.

[3] To whom correspondence should be addressed: 950 W. Walnut St., R2, Rm. 478, Indianapolis, IN 46202. Tel.: 317-278-6531; Fax: 317-278-5849; E-mail: khanna5@iupui.edu.

[4] The abbreviations used are: LCM, lacosamide; 5A mut, CRMP-2 mutant with 5 amino acid mutations to alanine; AB, affinity bait; CAD, catecholamine A differentiated; CR, chemical reporter; CRMP-2, collapsin response mediator protein; DIV, days *in vitro*; EGFP, enhanced green fluorescent protein; VGSC, voltage-gated sodium channel; (*R*)-LCM, *R*-enantiomer of LCM; MPL, 1-methyl-2-pyrrolidinone; siRNA, small interference RNA; GFP, green fluorescent protein; E, embryonic day; ANOVA, analysis of variance.

development, in the adult CRMP-2 is also expressed in brain regions capable of axonal outgrowth, neurogenesis, and synaptic rearrangements (12). Such rearrangements of synaptic connectivity and aberrant neuronal growth have been observed in epilepsy (13). At least two studies have reported altered CRMP-2 levels in epilepsy. The first showed a decrease in CRMP-2 levels in brains from patients with mesial temporal lobe epilepsy that was refractory to treatment (14). The second reported decreased CRMP-2 levels in thalamuses of mice with absence seizures (15). However, the mechanism by which CRMP-2 contributes to the pathophysiology of epilepsy is unclear. One hypothesis is that LCM, by binding to CRMP-2, may prevent the aberrant synaptic connectivity and/or rearrangements seen in epilepsy.

In addition to these classically defined roles, we recently showed that CRMP-2 binds to voltage-gated calcium channels and directly affects transmitter release in dorsal root ganglion (16) and hippocampal neurons (17, 18), suggesting the possibility that CRMP-2 may modulate the activity of other ion channels. In particular, because initial reports of weak binding at the Na^+ channel site 2 (*i.e.* 10 μM = 25% inhibition of [^{3}H]batrachotoxin binding), it is becoming increasingly clear that the primary clinical target of LCM is the VGSC (6, 7). Nine distinct VGSC isoforms (Nav1.1–1.9) have been identified whose heteromultimeric structure consists of a single pore-forming α-subunit (~240 kDa) arranged in six transmembrane segments (S1–S6) within four domains (19, 20). Studies have suggested that alteration of the slow inactivated state, through interactions with S6 regions of VGSCs, could be clinically relevant in limiting the activity of neurons with abnormal activity. Both increases and decreases in levels of CNS enriched Nav1.2, -1.3, and -1.6 (as well as cardiac Nav1.5) isoforms have been reported following experimental seizures in animals and in human chronic epilepsy (21–23). Thus, changes in expression levels of lacosamide target proteins may have disease-modifying effects. For instance, a decrease in CRMP-2 coupled with an alteration in Na^+ channel isoform expression may necessitate changes in dosages required for antiepileptic effects.

In this study, we used whole cell patch clamp electrophysiology to investigate how molecular interaction of LCM with CRMP-2 affects biophysical properties of VGSCs in a model neuronal cell line. In addition, using molecular modeling of LCM-binding sites on CRMP-2 and expression of alanine mutations of these sites, we studied the effects of LCM on slow inactivation of VGSCs. We identify key residues within CRMP-2, which, when mutated, alter the effects of LCM on the fraction of Na^+ channels stabilized in a slow inactivated state. Thus, our results show that interactions between LCM and its target proteins are important determinants of its full mode of action.

EXPERIMENTAL PROCEDURES

Chemicals and Solutions—All reagents were purchased from Sigma unless otherwise indicated. Lacosamide (*R*-2-acetamido-*N*-benzyl-3-methoxypropionamide) was purchased from Cayman Chemicals (Ann Arbor, MI) or synthesized as described by us previously (1). A 100 mM solution was made up in 1-methyl-2-pyrrolidinone (MPL) and stored in small aliquots at −20 °C. The final concentration of MPL in physiological solutions was <0.01% (v/v). Lacosamide was applied onto the cells through a custom made Y-tube microperfusion system. A concentration of 100 μM LCM was used because it 1) represents <2 times the reported therapeutic plasma levels (~60 μM (8)), 2) is exactly the concentration used in N1E-115 mouse neuroblastoma cells (6), 3) is ~1.7-fold the reported value for half-maximal inhibition of spontaneous excitatory postsynaptic currents and inhibitory postsynaptic currents (24), and 4) is within the linear part of the dose response curve testing for effects of LCM on inactivation of two isoforms of Na^+ channels expressed in human embryonic kidney 293 cells (7).

CAD Cells—Catecholamine A-differentiated (CAD) cells were grown at 37 °C and in 5% CO_2 (Sarstedt, Newton, NC) in Ham's F-12/Eagle's minimum essential media (Amersham Biosciences), supplemented with 8% fetal bovine serum (Sigma) and 1% penicillin/streptomycin (100% stocks, 10,000 units/ml penicillin G sodium, and 10,000 μg/ml streptomycin sulfate) (25). Cells were passaged every 6–7 days at a 1:25 dilution.

Transfection—Adherent CAD cell cultures were transfected with cDNAs using Lipofectamine 2000 (Invitrogen) as per the manufacturer's instructions. We routinely achieved >90% transfection efficiencies in CAD cells transfected with this method. Typically, CAD cells were transfected with equal amounts of different cDNA constructs, and electrophysiology experiments were performed 2 days later.

Knockdown of CRMP-2 Expression by siRNA—Validated short interfering RNAs (siRNAs) against the rat CRMP-2 (5′-ACTCCTTCCTCGTGTACAT-3′) sequence (26) and controls (scrambled sequence with approximately the same percentage of GC but no sequence homology) were used for CRMP-2 knockdown (Invitrogen) in CAD cells as previously described (16, 17). Cells were incubated for 2 days with vector-siRNA or scramble siRNA (500 nM), and assessment of knockdown was by quantitative Western blot analysis.

Molecular Docking—The three-dimensional structure of CRMP-2 was obtained from the RCSB data bank (PDB code: 2GSE) (27). The Sybyl 8.0 suite of programs (Tripos Inc., St. Louis, MO) was used to extract a monomer from the CRMP-2 tetrameric structure. Sybyl was also used protonate the structure and to assign Gasteiger atomic charges. The AutoDock 4 molecular docking package (28) was used to predict the binding site and binding mode of lacosamide on the CRMP-2 complex. The MGLTools (v1.5.2) (29) was used to assign Gasteiger charges to the protein and to generate the structural file for docking. The binding box spanned the entire structure of CRMP-2. Affinity grids on the binding pocket were constructed using AutoGrid4 (28) with grid spacing of 0.375 Å. The structure of lacosamide was constructed and prepared for docking with the program Sybyl. A combination of rigid receptor and flexible ligand protocol was used in the docking process using AutoDock. Compound conformational space was explored employing the Lamarckian genetic algorithm. The maximum number of energy calculations was set to 1,000,000. We carried out a total of 100 docking runs of lacosamide on the surface of CRMP-2. Final docked structures were visualized and analyzed using Sybyl 8.0 and PyMOL version 1.0. Images were rendered using PyMOL.

Cloning LCM-binding CRMP-2 Mutants—Mutagenic primers were designed to introduce the correct base pair change into CRMP-2 (accession NM_009955.2) using Vector NTI Advance 10 (Invitrogen). Mutations inserted into the CRMP-2 cDNA (30) construct were produced using the QuikChange XL site-directed mutagenesis kit (Stratagene, La Jolla, CA) according to the manufacturer's protocol. Full details of the molecular cloning, including mutagenic primer information, are provided under "Methods" of the supplemental information.

Preparation of Soluble Rat Brain Lysates—Rat brains (male, Sprague-Dawley, Rockland Immunochemicals, Gilbertsville, PA) were Dounce-homogenized in 50 mM HEPES buffer (pH 7.4). The lysate was centrifuged at slow speed (1200 × *g* for 12 min at 4 °C) to remove debris. The resulting supernatant was then centrifuged at high speed (100,000 × *g* for 1 h at 4 °C). The supernatant from this high speed spin was collected and stored at −80 °C until use. Total protein concentrations were determined with the Bradford assay.

AB&CR Agents Labeling, Cycloaddition Reaction, and In-gel Fluorescence Scanning—Rat brain lysate (1 ml, 50 mM HEPES buffer (pH 7.4)) was passed through a NAP-10 column (Amersham Biosciences) to exchange buffer to an aqueous 50 mM HEPES buffer (pH 7.8). Lysate aliquots (50 μl of 2.2 mg/ml protein in 50 mM HEPES buffer (pH 7.8)) were treated with lacosamide affinity bait (AB, where AB is isothiocynate, NCS) and chemical reporter (CR, where CR is alkyne) compounds (10 μM) at room temperature (20 min). The modified lysates were sequentially treated with rhodamine-azide (50 μM), tris(2-carboxyethyl)phosphine (1 mM), Tris[(1-benzyl-1H-1,2,3-triazol-4-yl)methyl]amine (100 μM), and $CuSO_4$ (1 mM). Samples were then shaken and allowed to rotate using Roto-shake (8 rpm, Model SI-1100, Scientific Industries Inc., Bohemia, NY) at room temperature (1 h). Proteins were separated by 10% SDS-PAGE after addition of 4× SDS-PAGE loading buffer and visualized by in-gel fluorescence using a Typhoon 9400 scanner (Amersham Biosciences) with excitation at 555 nm and detection at 580 nm.

Immunoblot Analysis—This was performed as described previously (16, 17). Briefly, CAD cells were lysed in radioimmune precipitation assay lysis buffer containing 50 mM Tris-HCl, pH 8, 1% Nonidet P-40 (Nonidet P-40/Igepal), 150 mM NaCl, 0.5% sodium deoxycholate, and 1 mM EDTA and supplemented with freshly added protease inhibitors: 1 μg/ml leupeptin, 2 μg/ml aprotinin, 1 mM phenylmethylsulfonyl fluoride (Sigma) together with a protease inhibitor mixture (Roche Applied Science, Laval, Quebec). After rotating for 30 min at 4 °C to facilitate lysis, cells were pelleted at 21,000 × *g* for 10 min at 4 °C. The supernatant was collected, and the protein concentration was determined by the BCA assay (Thermo Fisher Scientific, Shelbyville, IN). Twenty micrograms of protein was separated by SDS-PAGE (4–12% polyacrylamide gradient gel) and electrophoretically transferred onto polyvinylidene difluoride membranes (Invitrogen) and assayed for the presence of CRMP-2 (1:1,000, Chemicon, Billerica, MA), GFP (1:10,000, Clontech, Mountain View, CA), NaV channels (1:200, Alomone Laboratories, Jerusalem, Israel), and β-tubulin (1:1000, Promega, Madison WI) proteins using specific antibodies (31). The membranes were blocked for 1 h in 5% skim milk powder in TBST (25 mM Tris-Cl, pH 8.0, 125 mM NaCl, 0.1% to 2% polyoxyethylene sorbitan monolaurate (Tween 20)) at room temperature. Primary antibody incubations were for 2 h at room temperature or overnight at 4 °C. Following incubations with primary antibody and secondary antibody (goat anti-rabbit or anti-mouse IgG horseradish peroxidase (1:10,000, Stressgen, Ann Arbor, MI)), blots were washed extensively in TBST and probed with Enhanced Chemiluminescence Western blotting substrate (Thermo Scientific) before exposure to photographic film.

Primary Cortical Neuronal Cultures—Primary cortical cultures containing both glia and neurons were prepared from embryonic day 18 (E18) Sprague-Dawley rats as described (32). Following an aseptic dissection of cerebral cortices, the olfactory bulb and meninges were removed, and cortices were minced and incubated for 20–25 min at 37 °C in papain solution (12 units/ml, Worthington, Freehold, NJ) containing Leibovitz L-15 medium (Invitrogen), 0.42 mg/ml cysteine (Sigma), 250 units/ml DNase 1 (type IV, Sigma), 25 mM $NaHCO_3$, penicillin (50 units/ml)/streptomycin (50 μg/ml), 1 mM sodium pyruvate, and 1 mg/ml glucose (Invitrogen). The enzymatically dissociated tissue was then rinsed twice with Hanks' balanced salt solution lacking Ca^{2+} and Mg^{2+}. After dissociation, the cells were gently washed by sequential centrifugation in Neurobasal medium containing either 2 mg/ml or 20 mg/ml bovine serum albumin and penicillin/streptomycin, glucose, pyruvate, and DNase1 (as above) and then plated on poly-D-lysine-coated plates at a density of ~2 hemispheres per three 24-well plates (or 2 million cells/ml). Cells were fed twice a week with Neurobasal growth medium (500 μl/well) containing 2% NuSerum, 2% B27 (or 2% NS21 (33)), supplemented with penicillin/streptomycin (100 units/ml, 50 μg/ml), 0.1 mM L-glutamine, and 0.4 mM L-glutamax (Invitrogen), and at DIV 3–5 they were treated with the mitotic inhibitor 5-fluorodeoxyuridine/uridine (20 μg/ml, Sigma) to eliminate the dividing glia from the cultures. Neuronal media was supplemented every 2 days following fluorodeoxyuridine/uridine treatment. The cultures were used for Sholl analysis measurements at 5 DIV.

Sholl Analysis of Dendritic Complexity—The complexity of dendrites emanating from low density cortical neurons, transfected with enhanced green fluorescent protein (EGFP) or wild-type/mutant CRMP-2-EGFP was assessed by Sholl analysis. This analysis was performed with ImageJ using an automated Sholl analysis plug-in, in which the soma boundary is approximated by an ellipsoid, and dendrite intersections are assessed at radial distances from the soma (34). The dendritic tree was examined in 10-μm increments. Processes arising from the soma or from higher border dendritic segments that were shorter than 3 μm were rejected, because they could not be distinguished from filopodia.

Electrophysiology—Whole cell voltage clamp recordings were performed at room temperature on CAD cells using an EPC 10 Amplifier (HEKA Electronics, Germany). Electrodes were pulled from thin-walled borosilicate glass capillaries (Warner Instruments, Hamden, CT) with a P-97 electrode puller (Sutter Instrument, Novato, CA) such that final electrode resistances were 1–2 MΩ when filled with internal solutions. The internal solution for recording Na^+ currents contained (in mM): 110 CsCl, 5 $MgSO_4$, 10 EGTA, 4 ATP Na_2-ATP, and 25 HEPES (pH 7.2, 290–310 mosM/l). The external solution con-

tained (in mM): 100 NaCl, 10 tetraethylammonium chloride, 1 $CaCl_2$, 1 $CdCl_2$, 1 $MgCl_2$, 10 D-glucose, 4 4-aminopyridine, 0.1 $NiCl_2$, 10 HEPES (pH 7.3, 310–315 mosM/liter). Whole cell capacitance and series resistance were compensated with the amplifier. Series resistance error was always compensated to be less than ±3 mV. Cells were considered only when the seal resistance was <3 MΩ. Linear leak currents were digitally subtracted by P/4.

Data Acquisition and Analysis—Signals were filtered at 10 kHz and digitized at 10–20 kHz. Analysis was performed using Fitmaster and origin8.1 (OriginLab Corp.). For activation curves, conductance (G) through Na^+ channels was calculated using the equation $G = I/(V_m - V_{rev})$, where V_{rev} is the reversal potential, V_m is the membrane potential at which the current was recorded, and I is the peak current. Activation and inactivation curves were fitted to a single-phase Boltzmann function $G/G_{max} = 1/\{1 + \exp[(V - V_{50})/k]\}$, where G is the peak conductance, G_{max} is the fitted maximal G, V_{50} is the half-activation voltage, and k is the slope factor. Additional details of specific pulse protocols are described in the results text or figure legends.

Statistical Analyses—Differences between means were compared by either paired or unpaired two-tailed Student's t tests or an analysis of variance (ANOVA) when comparing multiple groups (repeated measures whenever possible). With the ANOVA, if a significant difference is determined, then a Dunnett's or Tukey's post-hoc test was performed. Data are expressed as mean ± S.E., with $p < 0.05$ considered as the level of significance.

RESULTS

LCM Binds to CRMP-2 in Rat Brain Lysate—Although lacosamide has been suggested to bind to CRMP-2 in a radioligand binding assay (8), a site of interaction has never been identified. Using a chemically modified lacosamide harboring "affinity bait" (AB) and "chemical reporter" (CR) moieties, we recently demonstrated lacosamide AB&CR labeling of expressed as well as endogenous CRMP-2 in mouse brain lysate (9). Here, we tested if lacosamide AB&CR adduction could be competed off using excess (*R*)-lacosamide. Adult rat brain lysates were treated with AB (isothiocynate (NCS))-CR (alkyne) lacosamide for 20 min at room temperature in the absence or presence of increasing amounts of (*R*)-lacosamide, and the lysate mixture was reacted with a rhodamine-containing probe under Cu(I)-mediated cycloaddition conditions ($CuSO_4$, tris(2-carboxyethyl)phosphine). The reaction samples were fractionated by electrophoresis using a 10% SDS-PAGE gel and then analyzed for proteins labeled by the AB&CR agents by in-gel fluorescence using a typhoon scanning laser (emission 532 nm, absorption 580 nm) (Fig. 1*A*). This strategy resulted in labeling of a protein of ~62 kDa, consistent with the predicted molecular weight of CRMP-2 (10) (Fig. 1*A*, *lane 1*). The intensity of this band was significantly reduced upon titration of (*R*)-lacosamide (Fig. 1*A*, *lanes 2* and *3*). Although other proteins were labeled with AB-NCS lacosamide, CRMP-2 and 1 other protein (Fig. 1*A*, *arrowhead*) showed a competitive displacement by excess (*R*)-lacosamide. These results demonstrate that (*R*)-lacosamide can selectively bind to CRMP-2 in rat brains.

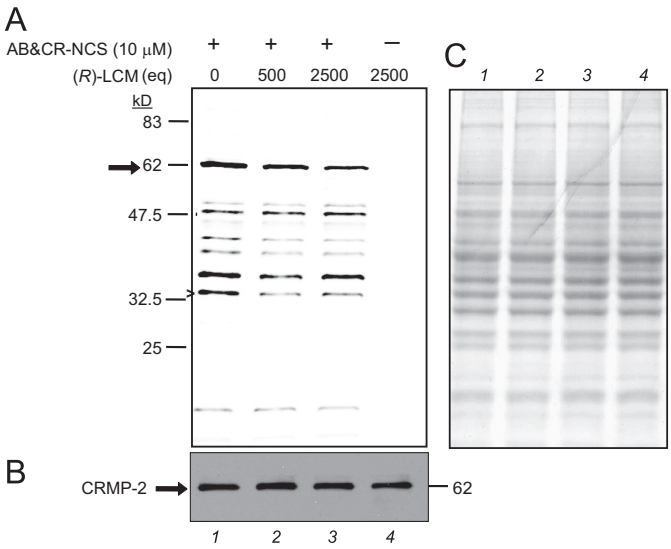

FIGURE 1. **(*R*)-Lacosamide binds to CRMP-2 in rat brain lysates.** *A*, *in vitro* labeling of endogenous CRMP-2 in rat brain lysate. Rat brain lysate (~110 μg) was incubated with the affinity bait isothiocyanate and chemical reporter (AB-NCS&CR; 10 μM) LCM for 20 min at room temperature in the absence or presence of increasing amounts of LCM with 500 equivalent (*eq*) amounting to 5 mM LCM. AB&CR agent-labeled proteins were detected by in-gel fluorescence scanning after Cu(I)-mediated cycloaddition to a rhodamine-azide reporter probe. An *inverted black and white image* is presented. *B*, CRMP-2 protein was detected by Western blot analysis using an anti-CRMP-2 antibody. *C*, a *gray scale image* of the Coomassie Blue-stained gel in *A* showing equal loading of proteins in the various samples. Representative results from a total of three experiments are shown. Molecular mass markers are indicated in kilodaltons.

LCM Affects Na^+ Currents in CAD Cells—Having demonstrated LCM adduction of CRMP-2, we next tested if manipulations of CRMP-2 expression in CAD cells could alter the effects of LCM on its primary clinical target, VGSCs. Using the whole cell patch clamp configuration, the effects of LCM on VGSCs in the presence of overexpressed CRMP-2 were examined. CAD cells were chosen, because they 1) provide a background easily amenable to genetic manipulation, 2) are of neuronal origin, and 3) express endogenous tetrodotoxin-sensitive Na^+ currents (25). Current-voltage relationships in control EGFP or CRMP-2-EGFP-expressing CAD cells were examined by the application of 15-ms step depolarizations ranging from −70 mV to +80 mV (in +10-mV increments) from a holding potential of −80 mV (Fig. 2*A*). The transient inward current in CAD cells activated between −40 and −30 mV and reached its peak at 0 to +10 mV (supplemental Fig. S1). Peak inward Na^+ currents were measured and expressed as peak current density (pA/picofarad (pF)) to account for variations in cell size. Control EGFP-expressing CAD cells exhibited a peak current density of −42.8 ± 4.7 pA/pF ($n = 6$), whereas CRMP-2-EGFP-expressing CAD cells had a density of −51.5 ± 3.6 pA/pF ($n = 8$). The peak densities were not significantly different ($p = 0.16$, Student's t test). The endogenous Na^+ currents in control EGFP-expressing CAD cells were fully blocked by 100 nM tetrodotoxin (data not shown). Application of 100 μM LCM resulted in a 20–40% reduction in peak Na^+ current observed in EGFP- and CRMP-2-EGFP-expressing cells. Inhibition of Na^+ currents was not accompanied by changes in reversal potential, half-maximal activation, and slope parameters (see Fig. 5) for either transfected condition in the presence or absence of LCM.

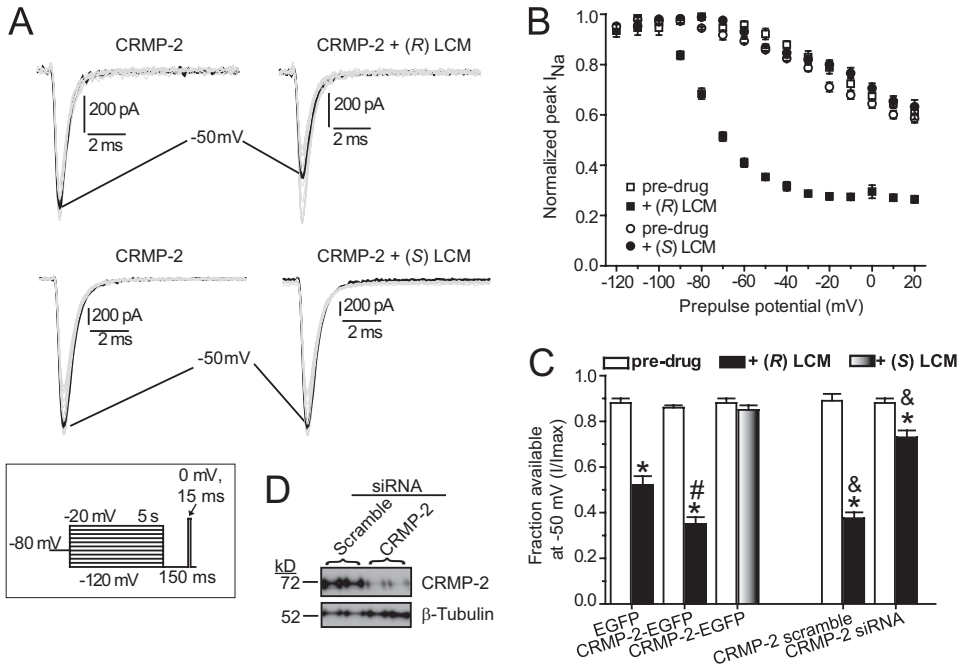

FIGURE 2. **Enantioselective modification of CRMP-2 by LCM affects steady-state slow inactivation state of Na$^+$ currents in CAD cells.** *A*, currents were evoked by 5-s prepulses between −120 mV and −20 mV, and then fast inactivated channels were allowed to recover for 150 ms at a hyperpolarized pulse to −120 mV. The fraction of channels available at 0 mV was analyzed. Representative current traces are from a CRMP-2-EGFP-overexpressing CAD cells in the absence (*left traces*) or presence (*right traces*) of LCM treatment. The *black trace* in each *panel* represents the current at −50 mV. *B*, summary of steady-state slow activation curves for CAD cells transfected with CRMP-2-EGFP before and after application of (*R*)- or (*S*)-LCM (100 μM). CRMP-2 overexpression blocked the development of LCM-induced slow inactivation, which was observed in EGFP-overexpressing neurons treated with LCM. *C*, summary of the fraction of current available at −50 mV for CRMP-2-expressing CAD cells in the absence or presence of (*R*)- or (*S*)-LCM (100 μM). (*R*)-, but not (*S*)-, LCM significantly reduced the fraction of current available at −50 mV (*, $p < 0.05$, Student's *t* test). Data are from 7–9 cells per condition. *D*, Western blot analysis with a CRMP-2 antibody showing successful (>90%) knockdown of CRMP-2 protein in CAD cells transfected with CRMP-2 siRNA compared with those transfected with scramble siRNA for 2 days. Under the same conditions, the expression the β-tubulin protein was unchanged. Duplicate lanes are from separate experiments.

These results show that CAD cells express typical tetrodotoxin-sensitive VGSCs that are sensitive to LCM.

CRMP-2 Overexpression Does Not Affect Steady-state Fast Inactivation—To test the ability of overexpressed CRMP-2 to affect fast inactivation in the absence or presence of LCM, we used a protocol (see Fig. 6) designed to accumulate channels in a fast-inactivated state, as previously described (6). Cells were held at −80 mV, stepped to inactivating prepulse potentials ranging from −120 to −10 mV (in 10-mV increments) for 500 ms, before stepping the cells to 0 mV for 20 ms to measure the available current. A 500-ms conditioning pulse was used, because it allows all of the endogenous channels to transition to a fast-inactivated state at all potentials assayed. To negate any possible effects of time-dependent shifts in the voltage dependence of fast inactivation, comparisons were always made on data obtained 3 min after establishing whole cell recording configuration from cells in the absence of drug with data recorded 3 min after establishing the whole cell recording configuration from cells in the presence of LCM. Steady-state inactivation curves of Na$^+$ currents from EGFP- and CRMP-2-EGFP-overexpressing CAD cells were well fitted with a single Boltzmann function ($R^2 > 0.9987$ for both). The $V_{½}$ value for inactivation for control EGFP-expressing CAD cells was −68.0 ± 0.7 mV ($n = 7$), which was not different from CRMP-2-EGFP-overexpressing CAD cells (−66.2 ± 1.3 mV, $n = 6$, $p > 0.05$; see Fig. 6, *C* and *D*). No statistically significant shifts in the voltage dependence of inactivation were observed in either condition in the presence of 100 μM LCM ($V_{½}$: EGFP plus LCM, −67.2 ± 0.5 mV, $n = 7$; CRMP-2-EGFP plus LCM, −69.5 ± 0.9 mV, $n = 5$; $p > 0.5$). The slopes (*k*) of the inactivation curves were also not affected by CRMP-2 overexpression or LCM treatment (see Fig. 6, *E* and *F*, $p > 0.5$).

(R)-, but Not (S)-, LCM Affects the Transition to a Slow Inactivated State of Na$^+$ Currents in CRMP-2 Overexpressing CAD Cells—LCM has been demonstrated to reduce VGSC availability by selectively enhancing the transition to a slow inactivated state of VGSCs (6, 7). Because our data indicated that LCM can affect Na$^+$ currents (data not shown), we tested the ability of LCM to modulate transition to a slow inactivated state in CRMP-2-EGFP-overexpressing CAD cells. Transfected CAD cells were held at −80 mV, conditioned to potentials ranging from −120 mV to −20 mV (in +10 mV increments) for 5 s, and then fast-inactivated channels were allowed to recover for 150 ms at a hyperpolarized pulse to −120 mV, and the fraction of channels available was tested by a single depolarizing pulse, to 0 mV, for 15 ms (Fig. 2*A*, *inset*). Addition of 100 μM LCM to CRMP-2-expressing cells significantly decreases the fraction of current available compared with those in the absence of LCM. For comparison, representative current traces at −50 mV are highlighted. This potential (−50 mV) was chosen, because 1) a large fraction of channels are undergoing steady-state inactivation, which involves contributions from slow and fast inactivating pathways (35, 36), wherein −50 is within the steep voltage dependence range for each, 2) it is near the resting membrane potential and approaching the action potential firing threshold for CNS neurons (37), where slow inactivation appears to be physiologically relevant during prolonged subthreshold depolarizations (38), and 3) changes in the Na$^+$ channel availability near −50 mV can impact the overlap of Na$^+$ current activating and inactivating under steady-state conditions (36, 39). Interestingly, the *S*-enantiomer of LCM did not reduce the available current (compare −50 mV traces in all families). The $V_{½}$ for steady-state slow inactivation, with a 5-s conditioning pulse, was −77.4 ± 1.2 mV ($n = 8$) in LCM-treated CRMP-2-EGFP-expressing cells compared with −61.1 ± 0.8 mV ($n = 7$) in LCM-treated EGFP-expressing cells ($p < 0.05$, Student's *t* test). At −50 mV, 0.35 ± 0.03% ($n = 8$) (calculated as 1 minus the

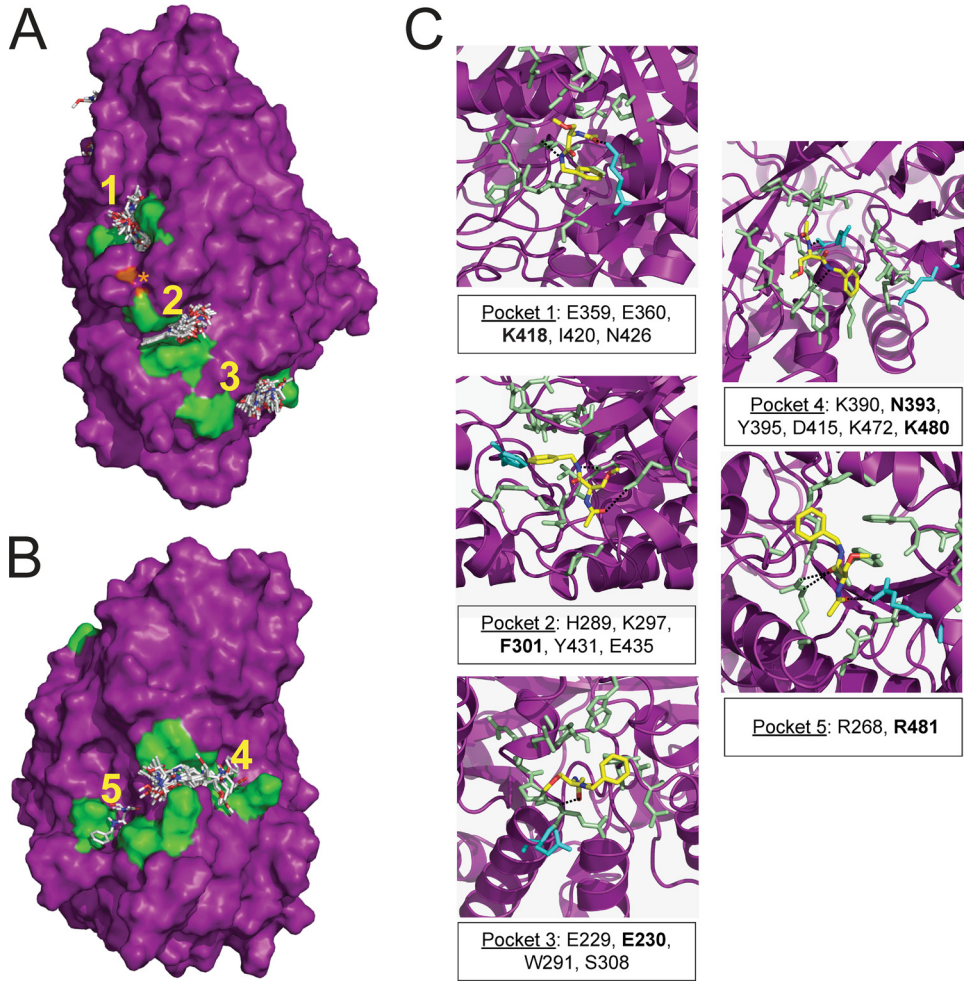

FIGURE 3. ***In silico* docking identifies five putative (*R*)-lacosamide binding pockets on CRMP-2.** *A* and *B*, surface representations of the three-dimensional structure of the CRMP-2 monomer (PDB code: 2GSE) with the locations of the putative binding pockets (*1–5*) highlighted in *green*. One or more LCMs bound to the five binding cavities within CRMP-2 are indicated. LCM is shown in *capped-sticks representation*. LCM is color-coded according to atom types (C, N, and O in *white*, *blue*, and *red*, respectively). The structure in *B* is rotated ~180° relative to that in *A*. *C*, an *enlarged view* of each of the five binding pockets. *C atoms* are shown in *yellow*. Only the predominant conformational state of LCM is shown in each pocket. The *asterisk* denotes the position of amino acid Ser-421 (*orange* residue) that is adjacent, but not predicted to be within coordinating range, of putative binding pocket 2. The residues coordinating LCM binding are indicated in *single amino acid letter code*. Residues in *bold* (shown in *blue*) indicate positions that were mutated to alanine. Hydrogen bonds are shown with *dashed lines*.

normalized I_{Na}) of the Na^+ current was available, suggesting a large fraction of the channels transitioned to a non-conducting (slow inactivated) state (Fig. 2*C*). These results demonstrate an enantioselective-specific modification of LCM on slow inactivation.

To further investigate if CRMP-2 manipulation affected Na^+ channel slow inactivation, we next asked if knockdown of CRMP-2 using siRNA against CRMP-2 (16, 17) would affect the mediated LCM transition of Na^+ channels to a slow inactivation state. We confirmed efficient and specific knockdown of CRMP-2 using siRNA with a >90% reduction in CRMP-2 protein (Fig. 2*D*). At −50 mV, 0.73 ± 0.05 (n = 5) of the Na^+ current was available in CAD cells transfected with CRMP-2 siRNA compared with 0.39 ± 0.04 (n = 5) in CAD cells transfected with scramble siRNA (Fig. 2*C*). Thus, CRMP-2 knockdown significantly reduces the fraction of channels present in a non-conducting (slow inactivated) state by ~60% compared with those in CRMP-2-overexpressing CAD cells (*i.e.* 1 − 0.73 or 27% *versus* 1 − 0.35 or 65%). Collectively, these results show that CRMP-2 manipulation impacts the ability of LCM to modulate the fraction of Na^+ channels existing in a slow inactivated state.

Molecular Docking Reveals Five Pockets for LCM Interaction with CRMP-2—Inferential data from preclinical reviews of LCM suggests that it may bind to CRMP-2 in a radioligand binding assay (8). However, a site of interaction has never been identified. In light of our results demonstrating reduction of Na^+ channel inhibition by LCM in CAD cells transfected with CRMP-2 siRNA, we wanted to identify putative sites of the interaction of LCM with CRMP-2. For this we turned to an *in silico* docking approach to identify potential binding sites that may sequester LCM making it more available and therefore more effective on Na^+ channels. A total of 100 docking runs were carried out over the entire surface of CRMP-2. The resulting binding mode of all 100 runs was visually analyzed. We found that LCM clustered at several binding pockets on the protein. Interaction energies for LCM bound to each of these cavities, and the number of hydrogen bonds mediated by the drug are listed in supplemental Table S1. The hydrogen bonds are illustrated in Fig. 3*C*. A total of five of these cavities showed more than one LCM bound (Fig. 3).

Single Alanine CRMP-2 Mutants of Putative LCM-binding Sites Express Well and Are Able to Modulate Dendritic Complexity—Using site-directed mutagenesis, we generated single alanine mutations of one or two amino acids in each pocket as identified in our docking studies. The selection of residues for each mutation was made based on visual analysis of each pocket. Residues whose side chains lined the cavity were considered to be most likely critical for binding. Preference was given to residues whose side chains were exposed to solvent and were not critical to maintain the structural integrity of the protein. An alanine mutant of amino acid Ser-421 in CRMP-2, not predicted to be within any of the pockets, was also generated (Fig. 3*A*, *orange residue*, *asterisk*). All of these CRMP-2 mutants were individually transiently transfected into CAD cells, resulting in the expression of full-length EGFP-fused proteins in immunoblot analyses (Fig. 4*A*).

To investigate if the mutant CRMP-2 proteins were substantially altered compared with wild-type CRMP-2, we measured

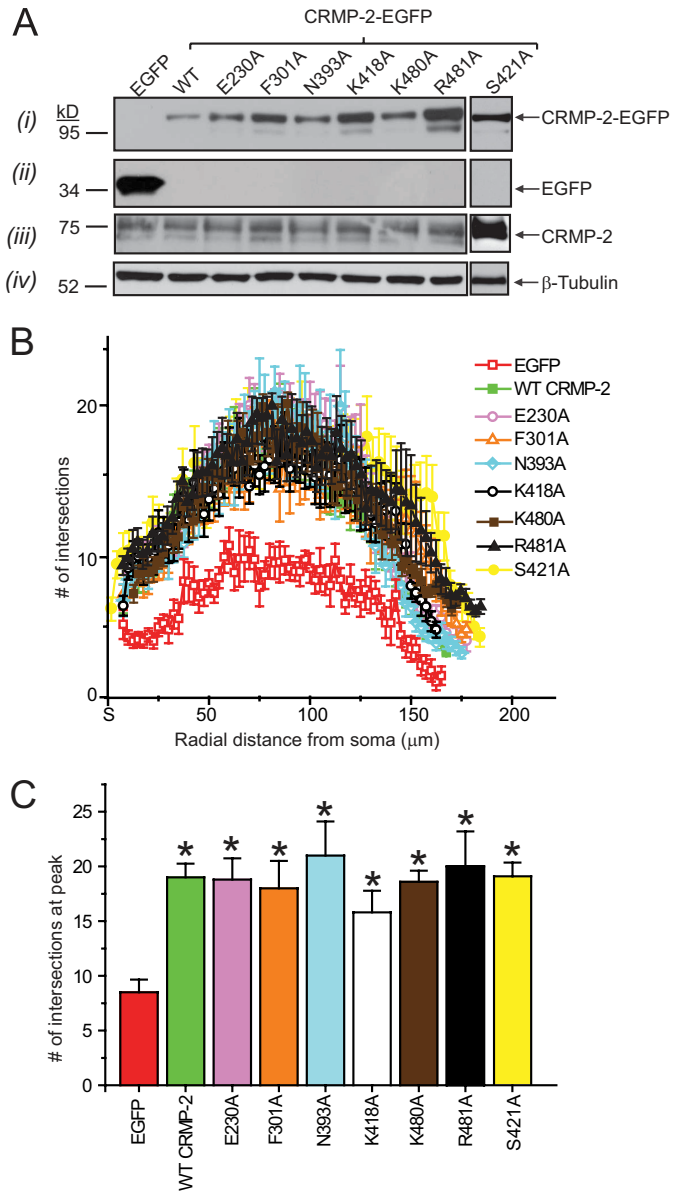

FIGURE 4. **Expression and functional characterization of lacosamide binding CRMP-2 alanine mutants in embryonic cortical neurons.** *A*, total protein lysates (20 μg each) from CAD cells expressing EGFP, CRMP-2-EGFP, or the various mutants were immunoblotted with antibodies against EGFP (*i* and *ii*), CRMP-2 (*iii*), and β-tubulin (*iv*). All CRMP-2-EGFP alanine mutants expressed well in CAD cells. Representative blots from three separate experiments are shown. Molecular mass standards are indicated on the *left* (kilodaltons). *B*, dendritic branching was calculated by Sholl analysis (41), which measures the number of neurites crossing concentric circles (intersections or branch points) at various radial distances from the cell soma. Sholl analysis of low density cultures of cortical neurons ($n = 10–12$ per condition) transfected at 3 DIV (and grown for 48 h) revealed a significant increase in the number of processes, reaching a peak of ~20 crossings at ~75–100 μm from the soma in wild-type and mutant CRMP-2-EGFP-transfected cells compared with EGFP transfected cells which reached a peak crossing of 8. *C*, summary of the average peak dendritic complexity for EGFP, wild-type CRMP-2EGFP, and mutant CRMP-2-EGFP transfected cortical neurons. A significant increase in neuritic complexity was seen in wild-type and all mutant CRMP-2-EGFP compared with EGFP-expressing (*, $p < 0.05$ *versus* EGFP at each distance between ~60 and 120 μm; Student's *t* test).

the effects of these proteins on neuronal differentiation and dendritic complexity. CRMP-2 is directly implicated in axon elongation and neuronal differentiation (12, 40). We compared the ability of the CRMP-2 mutants to increase dendritic complexity compared with wild-type CRMP-2 using Sholl analysis (41). This technique measures the number of neurites crossing concentric circles (denoted as intersections or branch points) at various radial distances from the cell soma. This consecutive-circles (cumulative intersection) analysis specifies dendritic geometry, ramification richness, and dendritic branching patterns. Sholl analysis was performed with ImageJ using an automated Sholl analysis plug-in, in which the soma boundary is approximated by an ellipsoid and dendrite intersections are assessed at radial distances from the soma (34). Sholl analysis of neonatal cortical neurons ($n = 10–12$ per condition), transfected with wild-type or CRMP-2 mutants (*i.e.* E230A, F301A, N393A, K418A, K480A, R481A, and S421A), at 3 DIV and analyzed at 5 DIV, revealed a significant increase in the number of processes compared with EGFP-transfected neurons. This increase reached a peak of ~20 crossings at ~75–100 μm from the soma in wild-type and all mutant CRMP-2-EGFP transfected neurons compared with EGFP-expressing neurons, which reached a peak complexity of ~8 crossings (Fig. 4*B*). A similar degree of increase in neuritic complexity was seen in wild-type CRMP-2-EGFP-transfected neurons compared with mutant CRMP-2-EGFP-transfected neurons (Fig. 4*C*), demonstrating that the CRMP-2 mutants were functionally unaffected, at least with respect to their ability to induce neurite outgrowth, by introduction of the individual alanine mutations.

Activation and Fast Inactivation Properties of Single Alanine CRMP-2 Mutants of Putative LCM-binding Sites Are Not Different from Wild-type CRMP-2—We next tested the effects of the CRMP-2 mutants on activation and fast inactivation. The CRMP-2 mutants did not alter the voltage dependence of activation of sodium currents in CAD cells, compared with wild-type CRMP-2, either under control conditions or during exposure to LCM (Fig. 5). Additionally, there were no changes in Na^+ current density in CAD cells transfected with any of the CRMP-2 mutants irrespective of LCM treatment (data not shown).

Steady-state fast inactivation curves of Na^+ currents from CAD cells overexpressing mutant CRMP-2-EGFP were fitted to a single Boltzmann function. The $V_{½}$ values for inactivation for all mutant CRMP-2 proteins expressed in CAD cells were similar to wild-type CRMP-2 in the presence or absence of LCM (Fig. 6, *C* and *D*). The slopes (k) of the inactivation curves were also not affected by mutant CRMP-2 overexpression or LCM treatment (Fig. 6, *E* and *F*).

The CRMP-2 Single Alanine Mutants Reduce the LCM-mediated Effects on the Ability of Endogenous Na^+ Channels to Transition to a Slow Inactivated State—Having established that 1) Na^+ channel activation and fast inactivation properties were not affected by introduction of single alanine CRMP-2 mutants into CAD cells and 2) a large (~65%) fraction of the Na^+ current in CAD cells transfected with wild-type CRMP-2 is in a slow inactivated state in the presence of LCM, we next tested if the fraction of channels existing in the slow inactivated state was altered in CAD cells overexpressing CRMP-2 mutants. For example, representative mutant (K480A) traces in the presence and absence of LCM display a conserved trend that LCM can still reduce the current elicited during the slow inactivation protocol. However, the fraction of Na^+ current available in

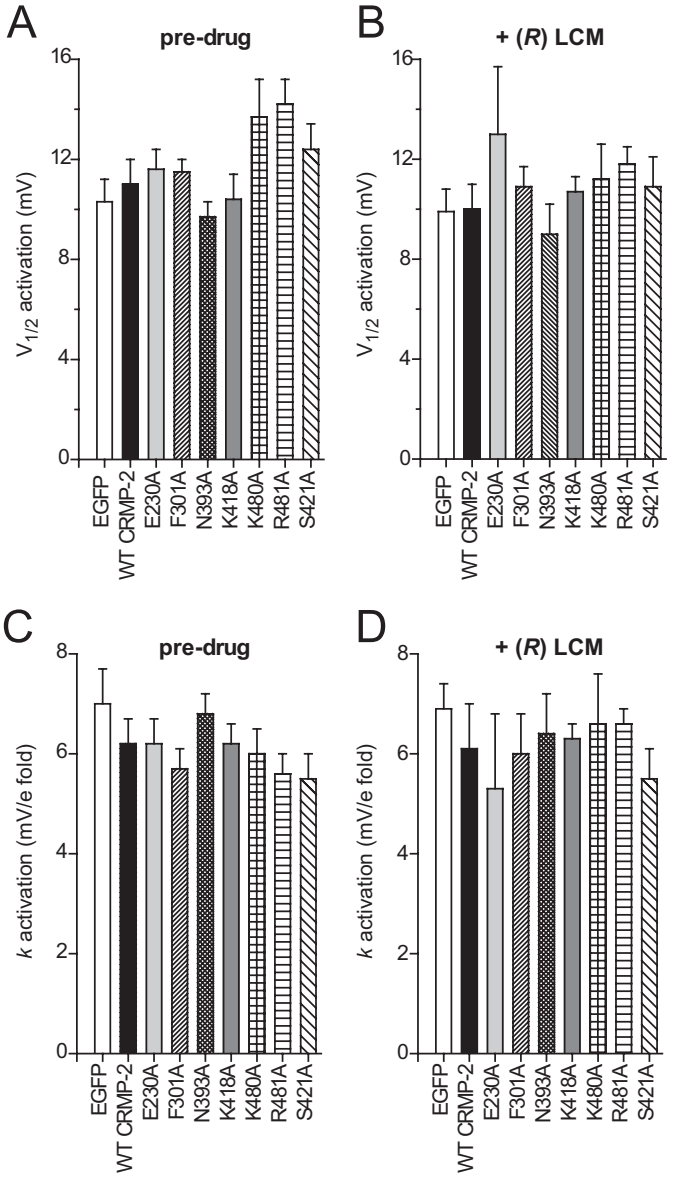

FIGURE 5. **Activation properties of Na^+ currents are not affected by LCM in CAD cells expressing wild-type or mutant CRMP-2 proteins.** Values for $V_{1/2}$, the voltage of half-maximal activation and the slope factors (*k*) were derived from Boltzmann distribution fits to the individual recordings and averaged to determine the mean (±S.E.) voltage dependence of activation. The $V_{1/2}$ (*A* and *B*) and *k* (*C* and *D*) of activation were not different between any of the conditions tested and irrespective of drug treatment ($p > 0.05$, one-way ANOVA).

CAD cells transfected with the single alanine mutants at −50 mV in the presence of LCM was increased by ~40–50% compared with wild-type CRMP-2-overexpressing CAD cells (Fig. 7*B*, #, $p < 0.05$ *versus* wild-type CRMP-2). There was no difference in the fraction of channels available in the presence of drug between the 6 single alanine mutants (Fig. 7*B*, *filled bars*). Notably, mutation of a CRMP-2 amino acid not predicted to be within any of the LCM binding pockets (*i.e.* S421A) did not change the fraction of Na^+ channels in a slow inactivated state compared with EGFP or wild-type CRMP-2-EGFP-overexpressing CAD cells (Fig. 7*B*, *hatched bar*, $p > 0.05$ *versus* both). However, the fraction of Na^+ channels in a slow inactivated state in CAD cells overexpressing S421A CRMP-2 was signifi-

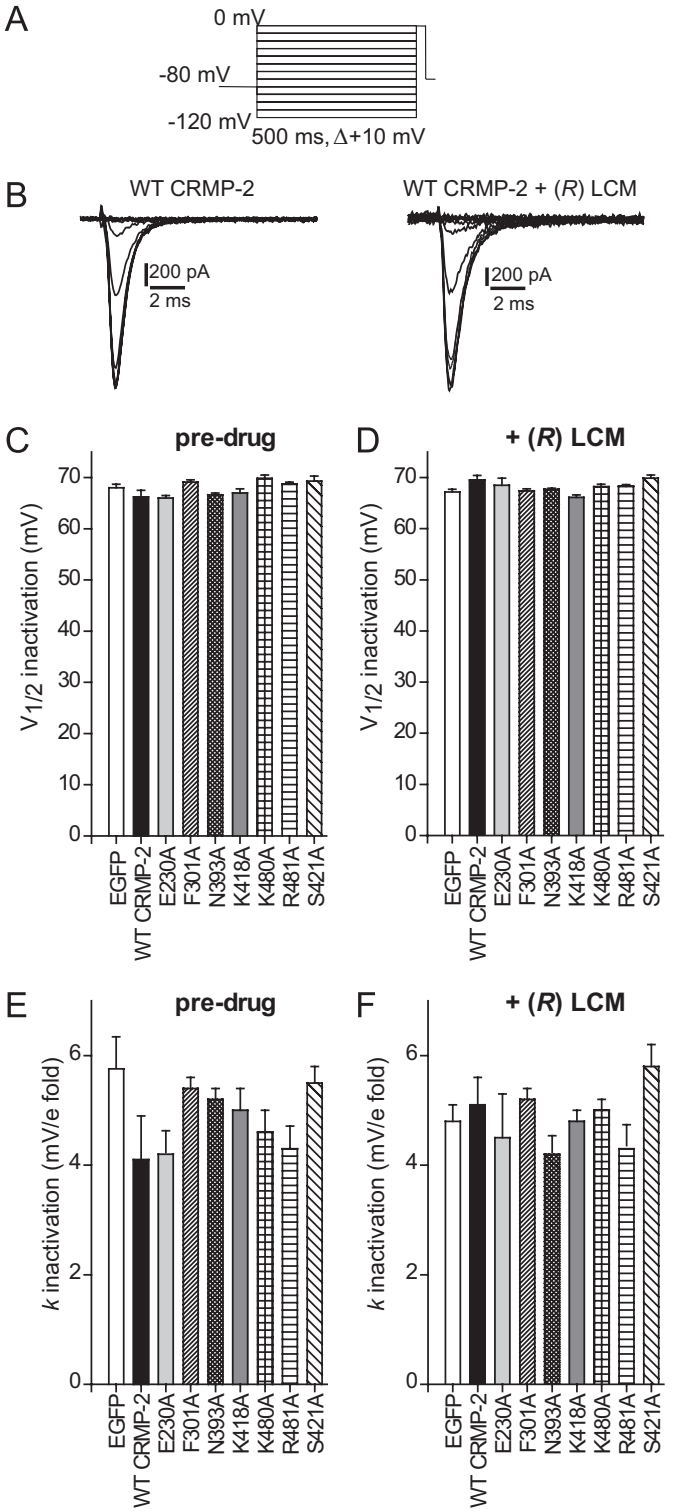

FIGURE 6. **Fast inactivation properties of Na^+ currents are not affected by LCM in CAD cells expressing wild-type or mutant CRMP-2 proteins.** *A*, voltage protocol for fast inactivation. *B*, representative current traces showing voltage-dependent fast inactivation of sodium currents from CAD cells expressing wild-type CRMP-2 in the absence (*left*) or presence (*right*) of 100 μM LCM. Values for $V_{1/2}$, the voltage of half-maximal inactivation, and the slope factors (*k*) were derived from Boltzmann distribution fits to the individual recordings and averaged to determine the mean (±S.E.) voltage dependence of steady-state inactivation. The $V_{1/2}$ (*C* and *D*) and *k* (*E* and *F*) of steady-state fast inactivation were not different between any of the conditions tested and irrespective of drug treatment ($p > 0.05$, one-way ANOVA).

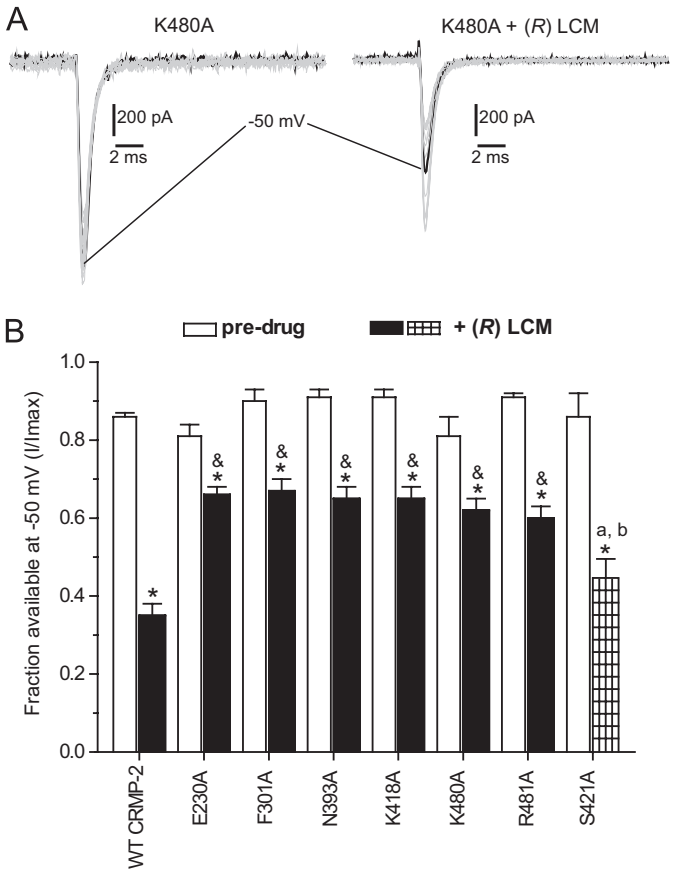

FIGURE 7. **(*R*)-Lacosamide increases the fraction of Na^+ current available in CAD cells expressing CRMP-2 mutants.** *A*, representative traces from CAD cells expressing K480A CRMP-2-EGFP in response to a voltage protocol (see *inset* in Fig. 2*A*) designed to measure slow inactivation. Current traces in the absence (*left traces*) or presence (*right traces*) of 100 μM LCM treatment are shown. The *black trace* in each *panel* represents the current at −50 mV. *Traces* are shown for the K480A only, because all other mutants behaved in a similar manner. *B*, summary of the average fraction of current available, at −50 mV, in the absence (*open bars*) and presence (*filled bars*) of LCM (n = 7–9 cells per condition). LCM decreased the fraction of current available compared with pre-drug values for wild-type (*WT*) and mutant CRMP-2 proteins (*, $p < 0.05$, ANOVA with Dunnett's post-hoc test). The fraction of current available in CAD cells expressing the various CRMP-2 mutants in the presence of LCM was significantly greater than that in wild-type CRMP-2 (&, $p < 0.05$, ANOVA with Dunnett's post-hoc test). In contrast, the fraction of current available in CAD cells expressing the S421A CRMP-2 mutant in the presence of LCM was not significantly greater than that in wild-type CRMP-2 (^{a}, $p = 0.0895$) but was significantly smaller than any of the other CRMP-2 mutants (^{b}, $p < 0.05$, ANOVA with Dunnett's post-hoc test).

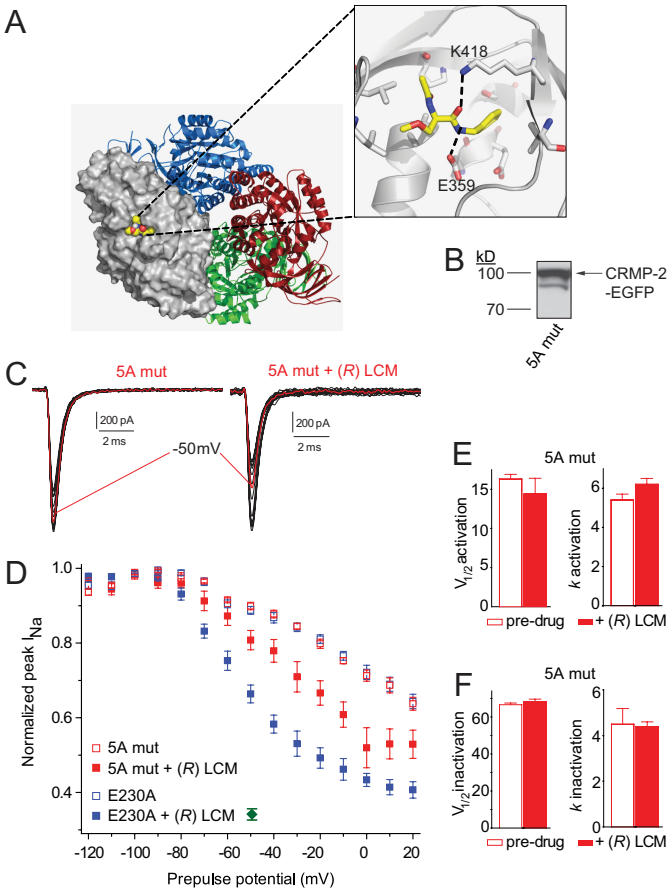

FIGURE 8. **A quintuplet alanine mutant of CRMP-2 reduces (*R*)-lacosamide-induced shift in slow inactivation of Na^+ currents in CAD cells.** *A*, three-dimensional structure of the CRMP-2 tetramer (PDB code: 2GSE). Each subunit within the tetramer structure is shown in a *different color*. The subunit used for the docking is shown in *gray surface representation*, whereas the remaining three are depicted in *blue*, *red*, and *green ribbon representation*, respectively. LCM is shown in a binding cavity within CRMP-2. The drug is depicted in *sphere representation*. A more detailed view is shown in the *right panel*. LCM is shown in *capped-sticks representation* along with the side chain or amino acids that delineate the binding cavity. The molecule is color-coded according to atom types (C, N, and O in *yellow*, *blue*, and *red*, respectively). The same color-coding is used for the amino acids in CRMP-2 except that carbon is shown in *gray*. *Dashed lines* are used to show hydrogen-bonding interactions. *B*, immunoblot analysis with an anti-EGFP antibody of the quintuplet CRMP-2 mutant harboring alanine mutations at amino acids Glu-360, Ser-363, Lys-418, Ile-420, and Pro-443 (*i.e.* 5A mut) in CAD cells. *C*, representative traces from CAD cells expressing the 5A mut in response to the slow inactivation voltage protocol shown in Fig. 3*A*. *Current traces* from the absence (*left traces*) or presence (*right traces*) of LCM treatment are shown. The *red trace* in each *panel* represents the current at −50 mV. *D*, summary of steady-state slow activation curves for CAD cells transfected with the single E230A (*blue symbols*) or the quintuplet 5A mut (*red symbols*) before and after application of LCM (100 μM). The 5A mut blocked the development of LCM-induced slow inactivation compared with the E230A mutant. For comparison, the fraction of channels available at −50 mV for wild-type CRMP-2 in the presence of LCM is shown as a *green diamond*. Values for $V_{1/2}$, the voltage of half-maximal activation and inactivation, and the slope factors (k) were derived from Boltzmann distribution fits to the individual recordings and averaged to determine the mean (±S.E.) voltage dependence of activation and steady-state inactivation. The $V_{1/2}$ and k of activation (*E*) or inactivation (*F*) were not affected by LCM treatment ($p > 0.05$, one-way ANOVA). Data are from 7–9 cells per condition.

cantly different from any of the other single alanine CRMP-2 mutants ($p < 0.05$, ANOVA with Dunnett's post-hoc test). These results 1) suggest that mutating CRMP-2 can impact the efficacy of LCM on VGSCs, in particular reducing the ability of LCM to enhance the transition to a slow inactivated state, and 2) identify key amino acids that can potentially coordinate binding of LCM, thus making it more available for action on Na^+ channels.

The CRMP-2 Quintuplet Alanine Mutant Further Reduces the LCM-mediated Effects on the Ability of Endogenous Na^+ Channels to Transition to a Slow Inactivated State—To identify the cavity that serves as the most likely binding site to LCM, we ranked the CRMP-2-LCM complexes using the Glide energy score (Schrodinger, Inc.), which approximates the binding affinity of the ligand to the complex. The Glide score was obtained by re-docking LCM to the five aforementioned sites using the Glide docking program (42). As shown in Fig. 8, the best score (−6.1 kcal/mol) was found to correspond at the site located near Lys-418. The other scores ranged from −4.9 kcal/mol to −3.8 kcal/mol. The phenyl ring of LCM is ensconced

into a cavity delineated by Glu-360, Ser-363, Ile-420, and Pro-443 (Fig. 8*A*, *box*). A lysine residue (Lys-418) that is located outside the cavity forms a hydrogen-bonding interaction with the carbonyl oxygen of the amide bond within lacosamide. Another hydrogen bond is seen between the amide nitrogen of LCM and a glutamic acid (Glu-359) in the binding site. Therefore, we created a quintuplet CRMP-2 mutant harboring alanine mutations at amino acids E360A, S363A, K418A, I420A, and P443A (designated 5A mut) to test the possibility that this mutant may contribute significantly to the LCM-mediated transition to a slow inactivation state observed in Na^+ channels. We verified that this mutant expressed normally (Fig. 8*B*) and was functionally similar to wild-type CRMP-2 in the dendritic complexity assay (data not shown).

Next, we examined activation and fast inactivation properties of Na^+ channels in CAD cells expressing the 5A mutant. The $V_{½}$ of activation and k values were similar irrespective of drug treatment (Fig. 8*E*) and were not significantly different values obtained from CAD cells overexpressing wild-type CRMP-2 or any of the single alanine mutants of CRMP-2. Similarly, we observed no differences in $V_{½}$ or k values of fast inactivation of Na^+ currents from cells overexpressing the 5A mutant irrespective of drug treatment (Fig. 8*F*).

Finally, to test the hypothesis that the mutated residues in CRMP-2 can modify the LCM-induced transition to a slow inactivated state of Na^+ channels, we measured slow inactivation using the same protocol as described earlier (see Fig. 2*A*, *inset*). The slow inactivation curve for CAD cells expressing the 5A mut, in the presence of LCM, was significantly right-shifted compared with wild-type CRMP-2 and the single alanine mutants. For comparison, the slow inactivation *versus* voltage curve for the single alanine mutant E230A is plotted along with the curve for the 5A mut (Fig. 8*D*). This illustrates a marked reduction in current available in the presence of drug for the 5A mut. At −50 mV, a voltage at which a large fraction of the channels are transitioning to an inactivated state, the fraction of current available in the presence of LCM is: 0.67 ± 0.02 ($n = 7$) for E230A *versus* 0.81 ± 0.02 ($n = 8$) ($p < 0.05$) for the 5A mutant. This indicates that at −50 mV, ~33% of the channels are inactivated/non-conducting in CAD cells expressing E230A, compared with ~19% in cells expressing the 5A mut and ~65% in cells expressing wild-type CRMP-2.

Collectively, these results suggest that amino acids Glu-360, Ser-363, Lys-418, Ile-420, and Pro-443 may form a binding pocket for LCM's interaction and that destruction of this pocket affects the slow inactivation state of Na^+ channels during LCM application.

DISCUSSION

In this study we investigated how CRMP-2, a recently identified target of LCM's action (9), affects LCM's modulation of its primary clinical target, the voltage-gated Na^+ channels. Fast inactivation was unaffected by LCM treatment. Enhancement of the entry of Na^+ channels into a slow inactivated state, a distinguishing feature of this drug, was increased by CRMP-2 overexpression. Molecular modeling revealed five pockets capable of binding LCM. Mutations of single amino acids within these pockets resulted in attenuation of LCM-induced enhancement of slow inactivation without any effects on activation or fast inactivation. A quintuplet alanine mutant of a putative high affinity cavity with CRMP-2 had the greatest effect on LCM-induced shift in slow inactivation of Na^+ channels, identifying this pocket as an important modifier of the main effect of LCM.

CRMP-2 Is a Bona Fide Target of LCM—Although inferential reviews have suggested a high affinity binding site for LCM on CRMP-2 (8), a site of interaction has not been identified. Using a chemical proteomics approach, we recently reported CRMP-2 interactions with AB&CR-LCM in mouse brain lysates as well as with recombinant CRMP-2 (9). CRMP-2 labeling was confirmed with differential stable isotope labeling followed by liquid chromatography-tandem mass spectrometry, revealing a selective ~80% increase in relative levels of CRMP-2 by (*R*)-, but not (*S*)-, LCM (9). In this study, we have extended these earlier findings by demonstrating labeling of CRMP-2 in rat brain soluble lysates. In addition, we also show that an isothiocyanate affinity bait version of LCM can be competitively displaced from CRMP-2 by addition of increasing amounts of unlabeled LCM. Importantly, even a considerably high amount (~25 mM) of LCM reduced CRMP-2 labeling by only ~50%, suggesting that CRMP-2 does not bind with a high affinity to LCM. A binding affinity for LCM could not be calculated from these experiments due to 1) issues with LCM solubility at higher concentrations and 2) labeling of bands other than CRMP-2 at higher concentrations of LCM. Despite these limitations, our results show that CRMP-2 is a *bona fide* target of LCM.

CRMP-2 Increases Extent of Enantiospecific Modification of Slow Inactivated State of Na^+ Channels—It has been previously shown that LCM selectively enhances sodium channel slow inactivation in a time- and voltage-dependent manner without affecting fast inactivation (6). LCM shifted the slow inactivation voltage curve to more hyperpolarized potentials and enhanced the maximal fraction of channels that were transitioning to a slow inactivated state. The slow inactivation process by lacosamide was stereoselective, with only the (*R*)-stereoisomer being active. Our results confirm these earlier findings of a LCM-induced shift in the fraction of Na^+ channels transitioning to a slow inactivated state (Fig. 3). However, LCM induced a shift of ~16 mV in the hyperpolarizing direction in CAD cells expressing CRMP-2 compared with those expressing EGFP control. At −50 mV, a physiologically relevant potential at which most of the channels are undergoing steady-state inactivation, $35 \pm 0.3\%$ ($n = 8$) of the Na^+ current was available in CRMP-2-expressing CAD cells *versus* $52 \pm 0.4\%$ ($n = 6$) in EGFP-expressing cells ($p < 0.05$, Student's t test). Consistent with this, siRNA that reduced CRMP-2 expression significantly reduced the enhancement of sodium channel slow inactivation by LCM. These results show that CRMP-2 levels modulate the ability of LCM to transition sodium channels to a non-conducting (slow inactivated) (Fig. 2*C*).

The CRMP-2-dependent changes in slow inactivation properties of Na^+ channels suggest that LCM-target protein interactions may have disease modifying effects. It is also plausible that interactions between Na^+ channels and CRMP-2 may directly affect the effects of lacosamide on both proteins. We

tested for this possibility by examining putative interactions between Na^+ channels and CRMP-2 in co-immunoprecipitation experiments. As shown in supplemental Fig. S2, no binding was observed in rat brain synaptosomes between the two proteins in the absence or presence of (*R*)- or (*S*)-LCM. Similar results were obtained in co-immunoprecipitations from CAD cells expressing CRMP-2 (data not shown). Although these results do not address if the proteins can bind directly, they show that Na^+ channels do not exist in a complex with CRMP-2. Nevertheless, because LCM can bind to CRMP-2 and affect the fraction of Na^+ channels in a slow inactivated state, it was important to investigate how CRMP-2 modulates Na^+ channel voltage-sensitive properties.

Molecular Docking Identifies Binding Pockets for LCM on CRMP-2—To identify putative LCM binding residues in CRMP-2 that may account for changes to the slow inactivated state of Na^+ channels, a molecular docking strategy was adopted. Following the iterative molecular docking of LCM on CRMP-2, 22 amino acids within 5 pockets were identified with more than one LCM bound. This approach has the advantage of selectively predicting, albeit *in silico*, binding sites capable of coordinating LCM. A limitation of this docking approach is that it does not take into account interactions of CRMP-2 with other proteins or interactions of LCM with other targets, which could lead to identification of CRMP-2 sites that might normally not be accessible or occupied by other targets.

Electrophysiological Characterizations of Alanine Mutants of Putative LCM-binding Sites Alters the Effect of LCM on Na^+ Channels—Guided by molecular docking and structure-based alignments, we first mutated positive charged or bulky aromatic residues to alanine. Because addition of LCM to CAD cells expressing wild-type CRMP-2 enhances the fraction of Na^+ channels transitioning to a slow inactivated state, we predicted that mutations in LCM binding pockets would alter the proportion of Na^+ channels entering the slow inactivated state. Indeed, our results demonstrated marked reduction in the enhancement of slow inactivation at −50 mV (Fig. 7). But how do mutations in CRMP-2 alter slow inactivation properties of Na^+ channels? One possibility is that the individual alanine mutations paradoxically increase binding of LCM to CRMP-2. If the LCM-binding site(s) on CRMP-2 is/are rigid and are dependent on the "state/conformation" of CRMP-2, then the native interaction may occur at a relatively restricted rate when a pool of LCM is present. Upon perturbation of the binding sites (with alanine scanning at important coordinating sites within different pockets), LCM may more readily and easily find a stable binding pocket on CRMP-2, reducing the amount of LCM available to modulate slow inactivation of Na^+ channels. Interestingly, the 5A mutant had the greatest effect on reducing the enhancement of slow inactivation by LCM. These data indicate that the CRMP-2 and its interaction with LCM play an important role in modulating the enhancement of Na^+ current slow inactivation by LCM.

CRMP-2: A Novel Modulator of Slow Inactivation in VGSCs?—Slow inactivation is a distinct inactivation process from fast inactivation. Slow enhancement can play an important role in regulating neuronal excitability by modulating sodium channel availability. Although the exact mechanism underlying slow inactivation is still unknown (43, 44), it is likely to involve conformational changes of the channel, including a rearrangement of the pore and domains II or IV (39, 44). Slow inactivation can be modulated by cellular factors and/or accessory subunits. For example, β1 subunit expression impedes slow inactivation of Nav1.4 channels (45), and second-messenger induced reductions in sodium channel availability seem to involve enhancement of a process that is indistinguishable from slow inactivation (46). The specific mechanism by which CRMP-2 and LCM modulate slow inactivation of sodium channels may be complex.

It was recently demonstrated that increased microtubule (*i.e.* tubulin) polymerization, caused by the anticancer drug taxol, can reduce the fraction of cardiac Na^+ channels that are slow inactivated (47). Because CRMP-2 has been shown to play a key role in cytoskeletal dynamics in growing axons (40, 48, 49) by binding to tubulin dimers and enhancing microtubule formation (49, 50), an intriguing possibility is that LCM targets the CRMP-2-tubulin interaction. We tested for this possibility by performing co-immunoprecipitations with β-tubulin and CRMP-2 antibodies from synaptosomes and cytosolic fractions treated with 100 μM LCM (supplemental Fig. S3*A*). There was an increase in both the phosphorylated and non-phosphorylated forms of CRMP-2 that were captured by the β-tubulin antibody in synaptosomes treated with LCM. Neither the low speed supernatant (S1) nor the high speed (S2) supernatant cytosolic fractions had any differences in the amount of co-immunoprecipitable CRMP-2. Similar results were observed in pulldown experiments with recombinant CRMP-2-GST protein (supplemental Fig. S3*B*). Although these results support the notion that LCM increases tubulin binding to CRMP-2, which brings about cytoskeletal changes leading to a reduction in the fraction of Na^+ channels in a slow inactivated state, they do not address if the increased association between tubulin and CRMP-2 is due to effects of LCM on CRMP-2 phosphorylation status or on tubulin itself. In light of a recent report demonstrating the ability of CRMP-2 to act as a GTPase-activating protein for tubulin (51), it is possible that LCM may target CRMP-2's GTPase-activating protein activity to change Na^+ channel slow inactivation. However, because the tubulin polymerization activity of CRMP-2 is believed to be determined by two distinct domains within CRMP-2 (49, 51) as well as an autoinhibitory region within the N terminus of CRMP-2, further studies are needed to examine if, and through which domain(s), LCM may act.

Although our data indicate that CRMP-2 levels can substantially alter the ability of LCM to modulate sodium channel activity, this modulation may be dependent on the isoform of Na^+ channel expressed. Isoforms Nav1.1, -1.2, -1.3, -1.6, and -1.7 have been reported to be expressed in embryonic hippocampal neurons at 3 DIV (52). We previously demonstrated differential effects of LCM on heterologously expressed Nav1.3, Nav1.7, and Nav1.8 channels (7). For example, there was 25-fold difference in IC_{50} values for inhibition by LCM following prolonged depolarization of Nav1.3 and Nav1.8 channels (7). Although we did not address the isoform(s) targeted by LCM in CAD cells, it is likely to be Nav1.1, -1.2, or -1.3, because these channels have been reported to be expressed in these cells

(53). Future studies are needed to examine the details of how CRMP-2 levels modulate the effects of LCM on specific sodium channel isoforms.

Collectively, the findings reported here indicate that the function of LCM is unique. Although initial pharmacological evidence has been presented on LCM function, the full mechanism of action of this drug remains elusive. Identifying the molecular determinants of LCM inhibition of sodium channels and the consequences of LCM-CRMP-2 interactions should aid in the development of novel therapeutics.

Acknowledgments—We thank Dr. May Khanna (Indiana University School of Medicine), Nicole Ashpole, and Omotore Eruvwetere and members of the Paul and Carole Stark Neuroscience Research Institute for helpful comments and stimulating discussions.

REFERENCES

1. Choi, D., Stables, J. P., and Kohn, H. (1996) *J. Med. Chem.* **39,** 1907–1916
2. Perucca, E., Yasothan, U., Clincke, G., and Kirkpatrick, P. (2008) *Nat. Rev. Drug Discov.* **7,** 973–974
3. Harris, J. A., and Murphy, J. A. (2009) *Ann. Pharmacother.* **43,** 1809–1817
4. Curia, G., Biagini, G., Perucca, E., and Avoli, M. (2009) *CNS Drugs* **23,** 555–568
5. Tilz, C., Resch, R., Hofer, T., and Eggers, C. (2009) *Epilepsia* **51,** 316–317
6. Errington, A. C., Stöhr, T., Heers, C., and Lees, G. (2008) *Mol. Pharmacol.* **73,** 157–169
7. Sheets, P. L., Heers, C., Stoehr, T., and Cummins, T. R. (2008) *J. Pharmacol. Exp. Ther.* **326,** 89–99
8. Beyreuther, B. K., Freitag, J., Heers, C., Krebsfänger, N., Scharfenecker, U., and Stöhr, T. (2007) *CNS Drug Rev.* **13,** 21–42
9. Park, K. D., Morieux, P., Salomé, C., Cotten, S. W., Reamtong, O., Eyers, C., Gaskell, S. J., Stables, J. P., Liu, R., and Kohn, H. (2009) *J. Med. Chem.* **52,** 6897–6911
10. Goshima, Y., Nakamura, F., Strittmatter, P., and Strittmatter, S. M. (1995) *Nature* **376,** 509–514
11. Wang, L. H., and Strittmatter, S. M. (1996) *J. Neurosci.* **16,** 6197–6207
12. Schmidt, E. F., and Strittmatter, S. M. (2007) *Adv. Exp. Med. Biol.* **600,** 1–11
13. Cavazos, J. E., and Cross, D. J. (2006) *Epilepsy Behav.* **8,** 483–493
14. Czech, T., Yang, J. W., Csaszar, E., Kappler, J., Baumgartner, C., and Lubec, G. (2004) *Neurochem. Res.* **29,** 2189–2196
15. Ryu, M. J., Lee, C., Kim, J., Shin, H. S., and Yu, M. H. (2008) *J. Neurochem.* **104,** 1260–1270
16. Chi, X. X., Schmutzler, B. S., Brittain, J. M., Wang, Y., Hingtgen, C. M., Nicol, G. D., and Khanna, R. (2009) *J. Cell Sci.* **122,** 4351–4362
17. Brittain, J. M., Piekarz, A. D., Wang, Y., Kondo, T., Cummins, T. R., and Khanna, R. (2009) *J. Biol. Chem.* **284,** 31375–31390
18. Wang, Y., Brittain, J. M., Wilson, S. M., and Khanna, R. (2010) *Commun. Integr. Biol.* **3,** 172–175
19. Goldin, A. L., Barchi, R. L., Caldwell, J. H., Hofmann, F., Howe, J. R., Hunter, J. C., Kallen, R. G., Mandel, G., Meisler, M. H., Netter, Y. B., Noda, M., Tamkun, M. M., Waxman, S. G., Wood, J. N., and Catterall, W. A. (2000) *Neuron* **28,** 365–368
20. Catterall, W. A. (2000) *Neuron* **26,** 13–25
21. Klein, J. P., Khera, D. S., Nersesyan, H., Kimchi, E. Y., Waxman, S. G., and Blumenfeld, H. (2004) *Brain Res.* **1000,** 102–109
22. Bartolomei, F., Gastaldi, M., Massacrier, A., Planells, R., Nicolas, S., and Cau, P. (1997) *J. Neurocytol.* **26,** 667–678
23. Whitaker, W. R., Faull, R. L., Dragunow, M., Mee, E. W., Emson, P. C., and Clare, J. J. (2001) *Neuroscience* **106,** 275–285
24. Errington, A. C., Coyne, L., Stöhr, T., Selve, N., and Lees, G. (2006) *Neuropharmacology* **50,** 1016–1029
25. Wang, H., and Oxford, G. S. (2000) *J. Neurophysiol.* **84,** 2888–2895
26. Nishimura, T., Fukata, Y., Kato, K., Yamaguchi, T., Matsuura, Y., Kamiguchi, H., and Kaibuchi, K. (2003) *Nat. Cell Biol.* **5,** 819–826
27. Deo, R. C., Schmidt, E. F., Elhabazi, A., Togashi, H., Burley, S. K., and Strittmatter, S. M. (2004) *EMBO J.* **23,** 9–22
28. Morris, G. M., Goodsell, D. S., Huey, R., and Olson, A. J. (1996) *J. Comput. Aided Mol. Des.* **10,** 293–304
29. Sanner, M. F. (1999) *J. Mol. Graph. Model.* **17,** 57–61
30. Tahimic, C. G., Tomimatsu, N., Nishigaki, R., Fukuhara, A., Toda, T., Kaibuchi, K., Shiota, G., Oshimura, M., and Kurimasa, A. (2006) *Biochem. Biophys. Res. Commun.* **340,** 1244–1250
31. Khanna, R., Li, Q., Bewersdorf, J., and Stanley, E. F. (2007) *Eur. J. Neurosci.* **26,** 547–559
32. Goslin, K., and Banker, G. (1989) *J. Cell Biol.* **108,** 1507–1516
33. Chen, Y., Stevens, B., Chang, J., Milbrandt, J., Barres, B. A., and Hell, J. W. (2008) *J. Neurosci. Methods* **171,** 239–247
34. Charych, E. I., Akum, B. F., Goldberg, J. S., Jörnsten, R. J., Rongo, C., Zheng, J. Q., and Firestein, B. L. (2006) *J. Neurosci.* **26,** 10164–10176
35. Rudy, B. (1978) *J. Physiol.* **283,** 1–21., 1–21
36. Hodgkin, A. L., and HUXLEY, A. F. (1952) *J. Physiol.* **116,** 497–506
37. Bean, B. P. (2007) *Nat. Rev. Neurosci.* **8,** 451–465
38. Do, M. T., and Bean, B. P. (2003) *Neuron.* **39,** 109–120
39. Vilin, Y. Y., and Ruben, P. C. (2001) *Cell Biochem. Biophys.* **35,** 171–190
40. Inagaki, N., Chihara, K., Arimura, N., Ménager, C., Kawano, Y., Matsuo, N., Nishimura, T., Amano, M., and Kaibuchi, K. (2001) *Nat. Neurosci.* **4,** 781–782
41. Sholl, D. A. (1953) *J. Anat.* **87,** 387–406
42. Halgren, T. A., Murphy, R. B., Friesner, R. A., Beard, H. S., Frye, L. L., Pollard, W. T., and Banks, J. L. (2004) *J. Med. Chem.* **47,** 1750–1759
43. Goldin, A. L. (2003) *Curr. Opin. Neurobiol.* **13,** 284–290
44. Ulbricht, W. (2005) *Physiol. Rev.* **85,** 1271–1301
45. Webb, J., Wu, F. F., and Cannon, S. C. (2009) *Pflugers Arch.* **457,** 1253–1263
46. Carr, D. B., Day, M., Cantrell, A. R., Held, J., Scheuer, T., Catterall, W. A., and Surmeier, D. J. (2003) *Neuron* **39,** 793–806
47. Casini, S., Tan, H. L., Demirayak, I., Remme, C. A., Amin, A. S., Scicluna, B. P., Chatyan, H., Ruijter, J. M., Bezzina, C. R., van Ginneken, A. C., and Veldkamp, M. W. (2010) *Cardiovasc. Res.* **85,** 691–700
48. Gu, Y., and Ihara, Y. (2000) *J. Biol. Chem.* **275,** 17917–17920
49. Fukata, Y., Itoh, T. J., Kimura, T., Ménager, C., Nishimura, T., Shiromizu, T., Watanabe, H., Inagaki, N., Iwamatsu, A., Hotani, H., and Kaibuchi, K. (2002) *Nat. Cell Biol.* **4,** 583–591
50. Arimura, N., Ménager, C., Kawano, Y., Yoshimura, T., Kawabata, S., Hattori, A., Fukata, Y., Amano, M., Goshima, Y., Inagaki, M., Morone, N., Usukura, J., and Kaibuchi, K. (2005) *Mol. Cell. Biol.* **25,** 9973–9984
51. Chae, Y. C., Lee, S., Heo, K., Ha, S. H., Jung, Y., Kim, J. H., Ihara, Y., Suh, P. G., and Ryu, S. H. (2009) *Cell. Signal.* **21,** 1818–1826
52. Mechaly, I., Scamps, F., Chabbert, C., Sans, A., and Valmier, J. (2005) *Neuroscience* **130,** 389–396
53. Castañeda-Castellanos, D. R., Cano, M., Wang, J. K., Corbett, A., Benson, D., Blanck, T. J., Thornhill, W. B., and Recio-Pinto, E. (2000) *Brain Res.* **866,** 281–285